

ON THE VORTEX IDENTIFICATION WITHIN A LINEAR BLADE CASCADE - AN EXPERIMENTAL RESEARCH

ERIK FLÍDR

Czech Aerospace Research Centre, Laboratory of High-Speed Aerodynamics, Beranových 130, 199 00 Prague - Letňany

correspondence: flidr@vzlu.cz

ABSTRACT. This paper deals with the identification of the individual vortical structures within a linear blade cascade based on H criteria. The experimental data obtained from the pressure measurement at the cascade outlet were evaluated by a standard procedure to obtain the velocity field in one plane. Then, the vorticity in the flow field was evaluated based on Crocco's theorem, and in the final step, the helicity density was calculated. The impact of the inlet flow angle on the velocity field as well as on the vortical structures was investigated. The effect of the value of the H threshold on the vortex identification is discussed in the last part of the paper.

KEYWORDS: Linear blade cascade, vortex identification, H criteria, experimental research, pressure measurements.

1. INTRODUCTION

The flow through a turbine is a complicated phenomenon that has not been fully understood yet. This type of flow is affected by many parameters, such as geometry, Mach number, and Reynolds number. The idealised case of this flow is the test case of the linear blade cascade, where the mentioned parameters can be investigated separately, both from experimental and theoretical points of view, in specialised laboratories. These investigations have been supplemented by numerical modelling in the past decades, thanks to the advancement in the field of computer simulations.

The topic of this paper is to identify the vortical structure in the linear blade cascade. Therefore, a brief description of its evolution will be given here. In a real machine, as well as in the linear blade cascade, an inlet boundary layer forms at the end-wall in front of the blades. This boundary layer separates at the so-called saddle point, discovered experimentally by Langston et al. [1]. The separated boundary layer rolls up into a horse-shoe vortex with two legs (pressure and suction). The suction leg attaches to the suction surface behind the leading edge of the blade. The precise position of this reattachment is dependent on many factors, such as the pressure ratio. The pressure leg is driven by the pressure gradient into the blade channel, consuming a low-momentum fluid from the end-wall boundary layer. This mechanism is responsible for the passage vortex formation. The passage vortex then moves along the suction side of the blade side by side with the suction leg of the horse-shoe vortex. This model of the vortices in the cascade was proposed by Langston [2].

However, the situation is much more complicated, as shown by Sieverding and Van de Bosche [3]. Two vortices interact, and as a result of this interaction, they wrap around each other. This explains some results

where the position of the vortices was not the same in all tested cases and, therefore, contradicted the Langston model. Many more models of the vortices in the blade cascades were introduced. More recently, Wang et al. [4] presented their model based on smoke visualisation. Articles reviewing this topic have also been published, see e.g., Sieverding [5], Langston [6], or Ligrani [7]. The effects of the main parameters (inlet flow angle, both Mach and Reynolds numbers) influencing the vortical structures in the cascade were investigated experimentally by Perdichizzi [8–10], Hodson and Dominy [11, 12], and many others. To sum up the results obtained from the vast number of researches performed in the past, it can be concluded that the increase of the studied parameter was responsible for a higher kinetic energy dissipation (KED) in the flow due to the larger vortical structures. These experimental results are in agreement with theoretical predictions given by Hawthorne [13, 14], Marris [15–19], or Lakshminarayana [20]. Note that all of these studies were not focused on a precise identification of the vortices. The visualisation techniques give only a qualitative image of the situation, meanwhile, other papers were focused on different topics, such as on the evaluation of KED. The vortices were identified from the vorticity in the flow. This approach is not entirely accurate as a definition of the vortex is still debated, see e.g. Wu et al. [21]. Because of that, a different approach for the identification of the vortex structures in the blade cascade was chosen here. It is based on the H criteria as described by Zhang and Choudhury [22].

The paper aims to identify vortex structures in the linear blade cascade as precisely as possible from a new perspective. This motivation stems from the earlier work of Flidr et al. [23], where the conventional approach for calculating the (KED) caused by the

vortex structures failed due to the flow separation on the suction surface of the blade. Therefore, this identification allows a more accurate evaluation of the flow within the blade cascades in the future.

2. EXPERIMENTAL APPARATUS, SETUP AND METHODS

2.1. WIND TUNNEL, BLADE CASCADE AND PRESSURE PROBE

The experiments were conducted in the VZLU Laboratory of High-Speed Aerodynamics Palmovka, using a closed-loop low-pressure aerodynamic wind tunnel where both Mach and Reynolds numbers could be independently varied. The flow was induced by a twelve-stage radial compressor driven by a DC motor. The Mach number was adjusted by controlling the rotational speed of the compressor, while the Reynolds number was modified by adjusting the stagnation pressure in the tunnel, achieved through a set of vacuum pumps. A condensed dryer was used to regulate the air humidity in the tunnel. The wind tunnel featured a relaxation chamber, where stagnation parameters of the flow, such as the pressure and temperature, were measured. To minimise fluctuation components of the velocity, the chamber's inlet was equipped with a screen. The inlet flow angle was manipulated using a movable pair of semi-shaped nozzles positioned in front of the cascade.

The cascade itself was assembled between two acrylic windows and contained 9 blades to ensure the periodicity of the flow at the cascade outlet. The span of the blades was $h = 100$ mm with a chord of $c = 50$ mm and a pitch-to-chord ratio of $t/c = 0.9$. The cascade, along with the control volume where the calculations were performed, is schematically shown in Figure 1. The coordinate system of the cascade is also depicted.

Five-hole pyramid pressure probe was used to measure the outlet flow field. The diameter of the tubes from which the probe was manufactured was 0.4 mm, therefore, the tip of the probe had dimensions of 1.2×1.2 mm. Although the tip of the probe was small, the dimensions of the probe holder were larger compared to the probe tip so the measurement position closest to the wall, where the measurement was performed, was 6 mm from the side wall of the test section.

2.2. PERFORMED EXPERIMENTS

The effect of the inlet flow angle was investigated for both constant similarity criteria, i.e., Reynolds and Mach numbers. The Reynolds number was $Re_{2, \text{is}} = 2.5 \times 10^5$, and the Mach number was $M_{2, \text{is}} = 0.4$. The inlet flow angles were then set to $\alpha_1 = -20^\circ, 5^\circ$, and 30° , corresponding to the underloaded, nominal, and overloaded regimes. The inlet flow angle $\alpha_1 = 0^\circ$ (not investigated in this paper) corresponds to an axial inlet flow angle. The tested cascade had a constant pitch-to-chord ratio of $t/c = 0.9$.

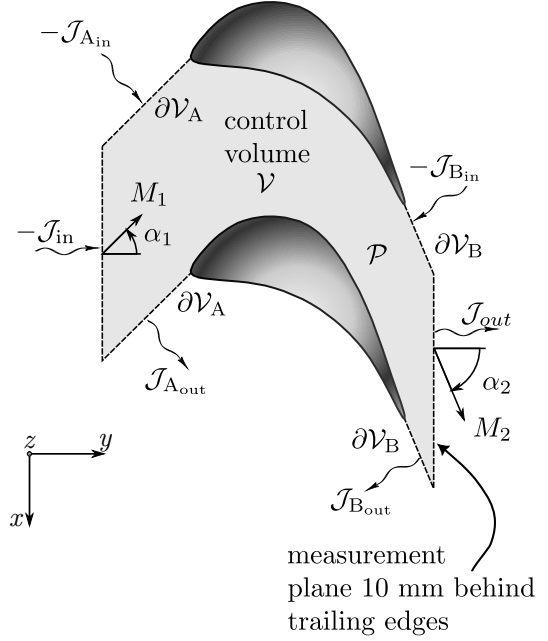


FIGURE 1. Scheme of the control volume.

2.3. METHODS

The measured data were processed using a standard procedure. Velocity vectors were calculated from the measured pressures using calibration matrices of the probe. From this velocity field obtained in one plane, the vorticity in the axial direction (y axis) was calculated directly as:

$$\omega_y = \frac{u_x^{(i+1),j} - u_x^{(i-1),j}}{z^{(i+1),j} - z^{(i-1),j}} - \frac{u_z^{i,(j+1)} - u_z^{i,(j-1)}}{x^{i,(j+1)} - x^{i,(j-1)}}, \quad (1)$$

where u_x and u_z represent the velocity components in the x (circumferential) and z (radial) directions, respectively. The remaining components of the vorticity vector were calculated using Crocco's theorem, expressed in the form:

$$\epsilon_{ijk} u_j \omega_k = \frac{1}{\rho} \partial_i p_0, \quad (2)$$

where ϵ_{ijk} is the Levi-Civita alternating tensor and p_0 is the stagnation pressure.

Having these, the helicity density was calculated as:

$$\mathcal{H} = u_i \omega_i. \quad (3)$$

Vortices were identified by the H criteria defined by Zhang and Choudhry [22] as:

$$H = \frac{\mathcal{H}}{|u_i| |\omega_i|}, \quad (4)$$

where the values of the H criteria lie within the range of $\langle -1; 1 \rangle$. The vortex can be identified as a region where this criterion reaches a certain threshold. For this paper, the chosen threshold value was $H \in \{ \langle -1; -0.6 \rangle \cup \langle 0.6; 1 \rangle \}$.

The local KED was defined as:

$$\zeta_i = 1 - \left(\frac{\lambda_2}{\lambda_{2, \text{is}}} \right)^2, \quad (5)$$

where λ_2 is the dimensionless velocity in the measured point and $\lambda_{2, \text{is}}$ is the isentropic dimensionless velocity obtained at the same point.

3. RESULTS AND DISCUSSIONS

3.1. VELOCITY DISTRIBUTIONS

Figures 2 to 4 represent distributions of the stream-wise velocity in the measurement outlet plane positioned 10 mm behind the trailing edges of the blades for three different inlet flow angles. The black contour lines in the figures illustrate the vortices identified by the H criterion.

The velocity reached values of $u_s \approx 120 \text{ m s}^{-1}$ in the wakes in the near-wall regions, where the vortices were identified, and rose up to $u_s \approx 140 \text{ m s}^{-1}$ at the blade mid-span in the channel, where the KED did not occur. It is noteworthy that the vortices identified by the H criterion did not always occupy the position with the lowest velocity, as seen in Figure 4. This discrepancy was influenced by the chosen value of the threshold H and will be discussed below. The position with the lowest velocity shifted more towards the blade mid-span with a higher inlet flow angle. This shift was caused by the movement of the vortices in the cascade towards the blade mid-span due to the higher centrifugal forces induced by the increased curvature of the channel.

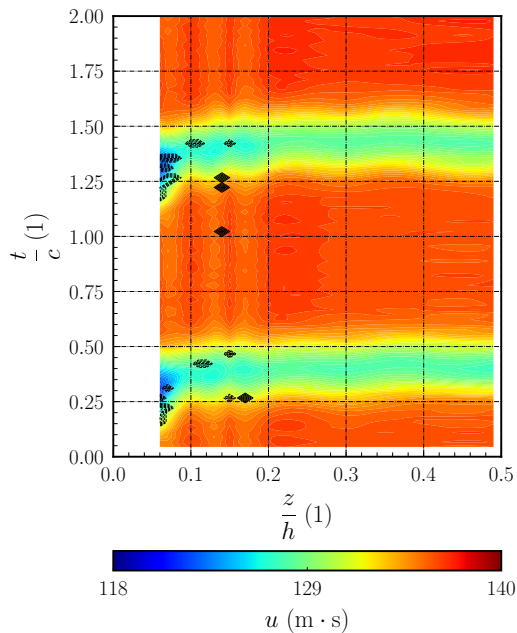


FIGURE 2. $\alpha_1 = -20^\circ$

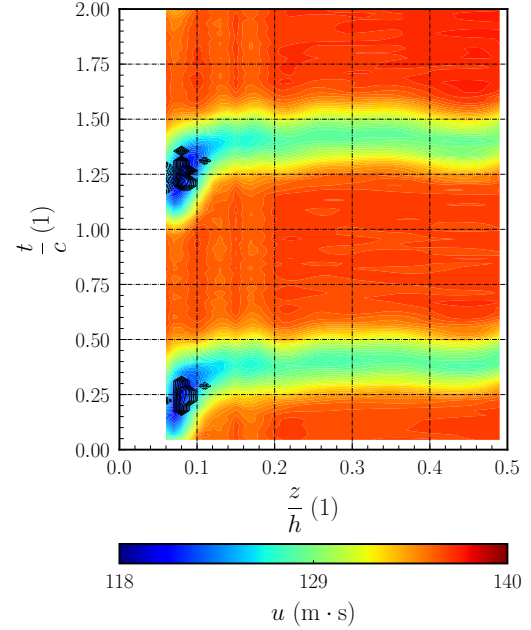


FIGURE 3. $\alpha_1 = 5^\circ$

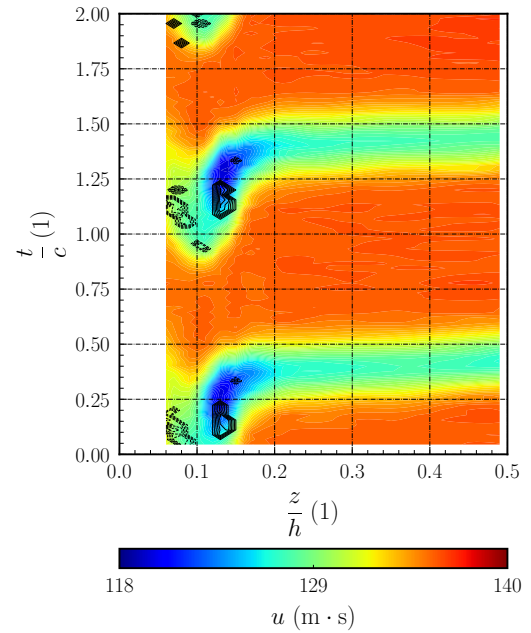


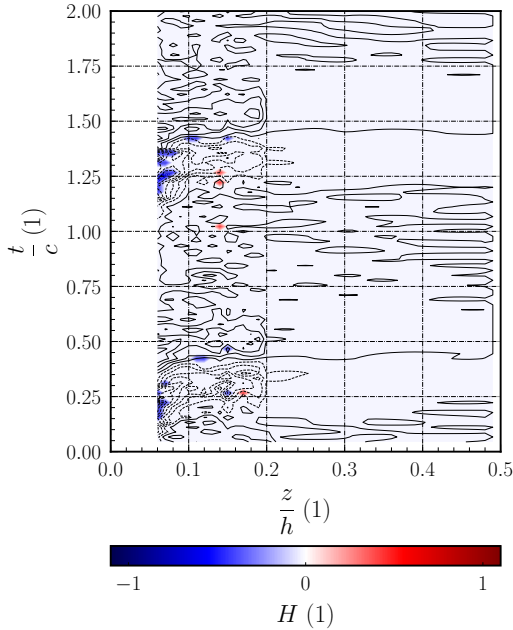
FIGURE 4. $\alpha_1 = 30^\circ$

3.2. VORTICES IDENTIFICATION

Figures 5 to 7 show vortices identified, again, by the H criterion along with the distributions of the stream-wise vorticity (black contour lines) in the same measurement plane. It is evident that the location of the vortices evaluated by the H criterion differed from the locations suggested by the higher stream-wise vorticity. The stream-wise vorticity was utilised in a past study [23] to localise and describe the evolution of the vortices. The qualitative results remained consistent

with the past study; that is, the vortices were more shifted towards the blade mid-span and enhanced in strength with increasing inlet flow angle due to larger centrifugal forces. However, their dimensions were overestimated. The problem arises from the fact that the vortex, as a flow structure, lacks a precise mathematical definition, as highlighted by Tang and Liu [24], and Zhang and Choudhry [22].

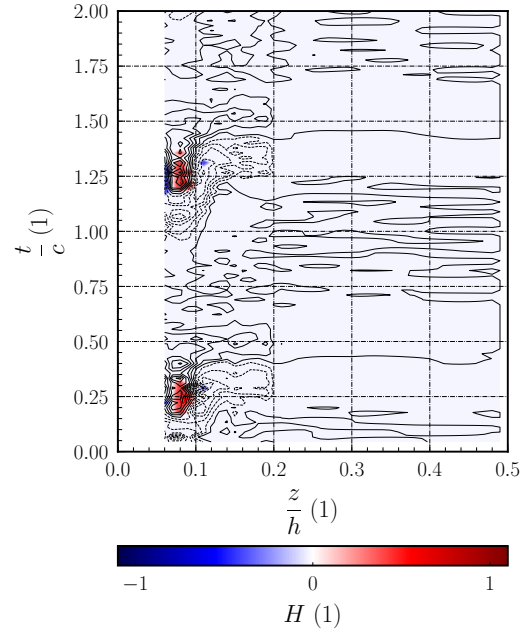
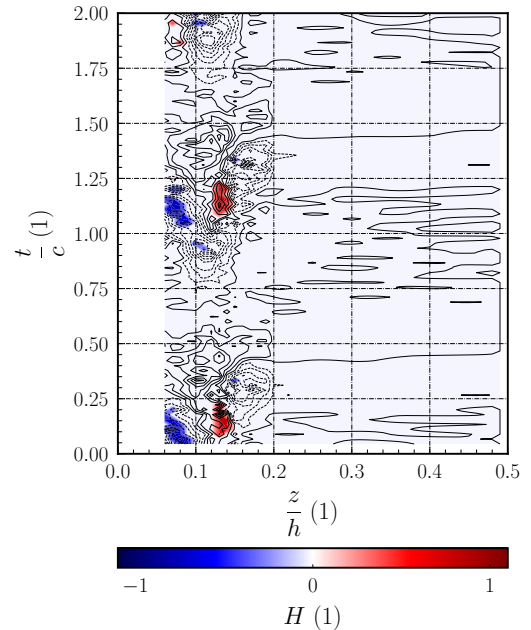
The positions of the vortices moved from the values $z/h \approx 0.06$ for $\alpha = -20^\circ$ up to $z/h \approx 0.14$ for $\alpha = 30^\circ$. Moreover, in the case of $\alpha = -20^\circ$, only small portions of the vortices further from the wall were observed. The red-colored vortices (corner vortices and suction side leg of the horse-shoe vortices) correspond with the vortices with clockwise rotations, meanwhile, the blue ones rotate in the opposite manner (passage vortices). It can be seen, that the vortices occupied approximately the same positions as the regions with the largest vorticity, however, their dimensions were considerably smaller.

FIGURE 5. $\alpha_1 = -20^\circ$

3.3. EFFECT OF THE H THRESHOLD ON THE VORTEX IDENTIFICATION

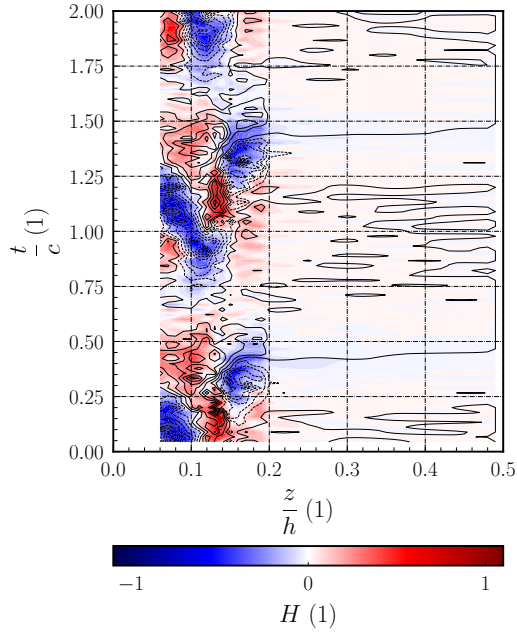
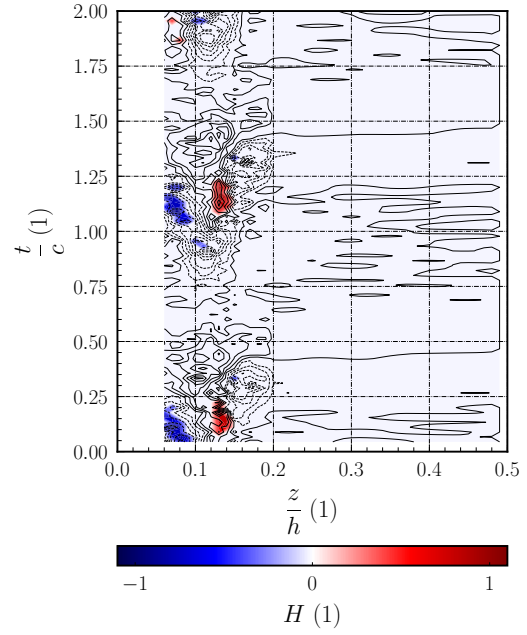
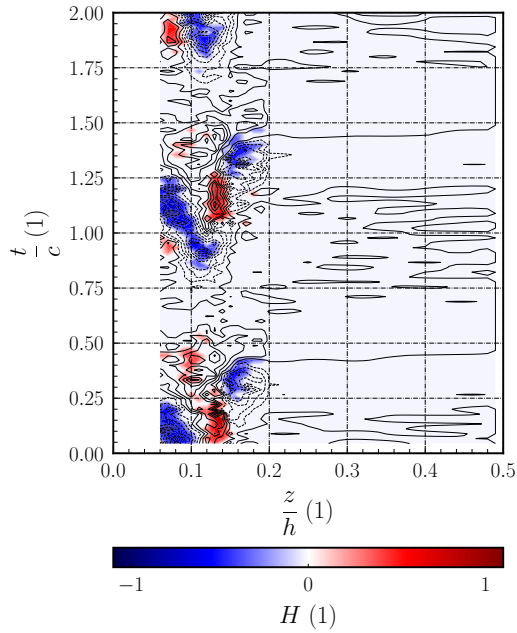
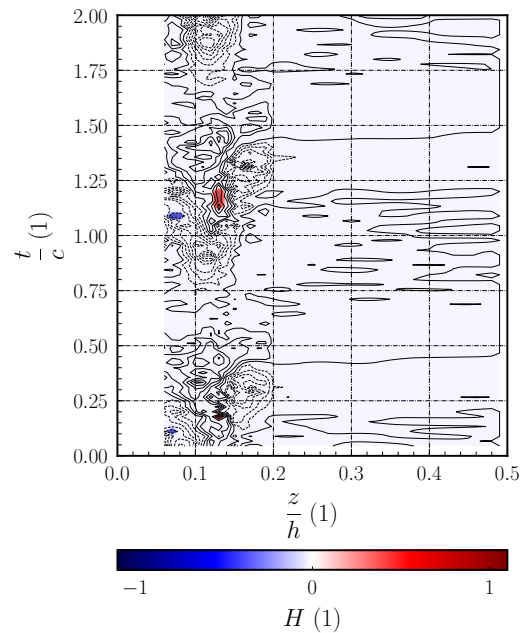
The effect of the value of the H threshold on the identification of the vortices is demonstrated in Figures 8–12.

It is evident that if there were no threshold ($H_{\text{threshold}} = 0$), the vortices identified in this way overlapped with the regions where the vorticity was nonzero (Figure 8). This definition of the vortex can be found in Wu, Ma, and Zhou [21], where vortices were defined as structures with nonzero vorticity. However, this definition includes even types of flow where the nonhelical movement of the fluid occurs,

FIGURE 6. $\alpha_1 = 5^\circ$ FIGURE 7. $\alpha_1 = 30^\circ$

such as the boundary layer on a flat plate. If helical motion has to be part of the vortex definition, such an approach has to be dismissed. Therefore, the H threshold must be chosen larger than zero.

Increasing the value of the threshold from zero up to 1 resulted in smaller identified vortices. In the limit of $H \rightarrow 1$, the identified vortex should be identical to its axis of rotation. This is demonstrated in Figure 12. However, this value was not reached in all cores of the vortices; therefore, all the vortex axes were not found.

FIGURE 8. $|H_{\text{threshold}}| = 0.0$ FIGURE 10. $|H_{\text{threshold}}| = 0.6$ FIGURE 9. $|H_{\text{threshold}}| = 0.3$ FIGURE 11. $|H_{\text{threshold}}| = 0.9$

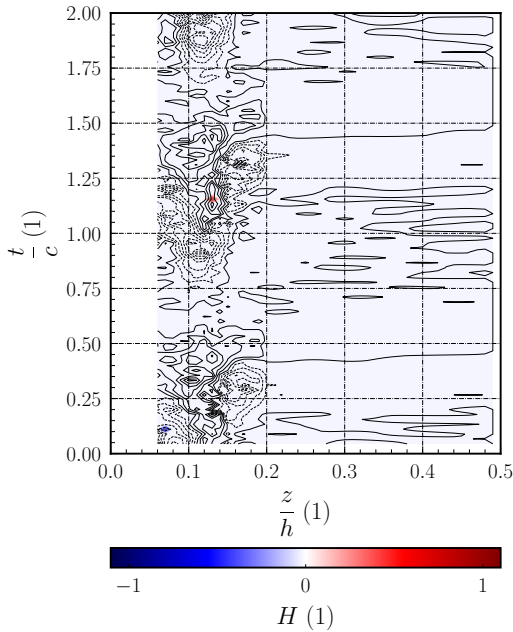
4. CONCLUSIONS

The paper focused on the identification of vortices in the linear blade cascade with a pitch-to-chord ratio of $t/c = 0.9$, maintaining a constant Reynolds number $Re_{2, \text{is}} = 2.5 \times 10^5$ and Mach number $M_{2, \text{is}} = 0.4$, while varying the inlet flow angle $\alpha_1 = -20^\circ, 5^\circ$, and 30° . It was demonstrated that the dimensions of the vortices depend on the value of the threshold H , which in the limit $H = 0$ collapsed into the same structures as if they were identified based on the nonzero vorticity

condition. Conversely, if the value of H was set equal to 1, the identified vortices corresponded with their axis of rotation.

A comparison of the vortex positions with distributions of the velocity field at the cascade outlet revealed that vortices occupied regions with the lowest velocities, where most of the kinetic energy of the flow was dissipated.

The evolution of the vortices with varying inlet flow angle aligned well with the theory of secondary

FIGURE 12. $|H_{\text{threshold}}| = 1.0$

flow in curved channels; specifically, with the increase of α_1 , the structures shifted more towards the blade mid-span due to larger centrifugal forces and were stronger.

In the following work, this vortex identification can be used to modify the methodology of evaluating the flow within the blade cascade. In particular, the KED is usually calculated as the superposition of the idealised 2D flow at the blade mid-span and the rest of the KED. However, to estimate the effect of the vortices correctly, their shapes should be taken into account. Therefore, the KED should be divided into three parts, specifically: the mid-span, end-wall, and vortex KED.

LIST OF SYMBOLS

c	Blade chord [mm]
h	Blade height [mm]
H	H criteria [1]
\mathcal{H}	Helicity density [m]
$M_{2,\text{is}}$	Isentropic outlet Mach number [1]
p	Pressure [Pa]
$Re_{2,\text{is}}$	Isentropic outlet Reynolds number [1]
t	Pitch [mm]
u_i	Components of velocity vector [m s^{-1}]
x, y, z	Cartesian coordinates [mm]
α_1	Inlet flow angle [$^\circ$]
ζ	Kinetic energy dissipation [1]
λ	Dimensionless velocity [1]
ρ	Density [kg m^{-3}]
ω_i	Components of vorticity vector [s^{-1}]
Indexes:	
0	Stagnation value

ACKNOWLEDGEMENTS

The work was not supported by any project, only by the author's curiosity.

REFERENCES

- [1] L. S. Langston, M. L. Nice, R. M. Hooper. Three-dimensional flow within a turbine cascade passage. *Journal of Engineering for Power* **99**(1):21–28, 1977. <https://doi.org/10.1115/1.3446247>
- [2] L. S. Langston. Crossflows in a turbine cascade passage. *Journal of Engineering for Power* **102**(4):866–874, 1980. <https://doi.org/10.1115/1.3230352>
- [3] C. H. Sieverding, P. Van den Bosche. The use of coloured smoke to visualize secondary flows in a turbine-blade cascade. *Journal of Fluid Mechanics* **134**:85–89, 1983. <https://doi.org/10.1017/S0022112083003237>
- [4] H. P. Wang, S. J. Olson, R. J. Goldstein, E. R. G. Eckert. Flow visualization in a linear turbine cascade of high performance turbine blades. *Journal of Turbomachinery* **119**(1):1–8, 1997. <https://doi.org/10.1115/1.2841006>
- [5] C. H. Sieverding. Recent progress in the understanding of basic aspects of secondary flows in turbine blade passages. *Journal of Engineering for Gas Turbines and Power* **107**(2):248–257, 1985. <https://doi.org/10.1115/1.3239704>
- [6] L. S. Langston. Secondary flows in axial turbines – A review. *Annals of the New York Academy of Sciences* **934**(1):11–26, 2001. <https://doi.org/10.1111/j.1749-6632.2001.tb05839.x>
- [7] P. Ligrani, G. Potts, A. Fatemi. Endwall aerodynamic losses from turbine components within gas turbine engines. *Propulsion and Power Research* **6**(1):1–14, 2017. <https://doi.org/10.1016/j.jprr.2017.01.006>
- [8] A. Perdichizzi. Mach number effects on secondary flow development downstream of a turbine cascade. *Journal of Turbomachinery* **112**(4):643–651, 1990. <https://doi.org/10.1115/1.2927705>
- [9] A. Perdichizzi, M. Ubaldi, P. Zunino. Reynolds stress distribution downstream of a turbine cascade. *Experimental Thermal and Fluid Science* **5**(3):338–350, 1992. [https://doi.org/10.1016/0894-1777\(92\)90079-K](https://doi.org/10.1016/0894-1777(92)90079-K)
- [10] V. Dossena, A. Perdichizzi, M. Ubaldi, P. Zunino. Turbulence measurements downstream of a turbine cascade at different incidence angles and pitch-chord ratios. In *Turbo Expo: Power for Land, Sea, and Air. Volume 1: Aircraft Engine; Marine; Turbomachinery; Microturbines and Small Turbomachinery*, p. V001T03A020. 1993. <https://doi.org/10.1115/93-GT-052>
- [11] H. P. Hodson, R. G. Dominy. The Off-design performance of a low-pressure turbine cascade. *Journal of Turbomachinery* **109**(2):201–209, 1987. <https://doi.org/10.1115/1.3262086>
- [12] H. P. Hodson, R. G. Dominy. Three-dimensional flow in a low-pressure turbine cascade at its design condition. *Journal of Turbomachinery* **109**(2):177–185, 1987. <https://doi.org/10.1115/1.3262083>

- [13] W. R. Hawthorne. Secondary circulation in fluid flow. *Proceedings of the Royal Society of London Series A Mathematical and Physical Sciences* **206**(1086):374–387, 1951. <https://doi.org/10.1098/rspa.1951.0076>
- [14] W. R. Hawthorne. Rotational flow through cascades part I – The components of vorticity. *The Quarterly Journal of Mechanics and Applied Mathematics* **8**(3):266–279, 1955. <https://doi.org/10.1093/qjmath/8.3.266>
- [15] A. W. Marris. The Generation of secondary vorticity in an incompressible fluid. *Journal of Applied Mechanics* **30**(4):525–531, 1963. <https://doi.org/10.1115/1.3636613>
- [16] A. W. Marris. On the generation of secondary velocity along a vortex line. *Journal of Basic Engineering* **86**(4):815–818, 1964. <https://doi.org/10.1115/1.3655961>
- [17] A. W. Marris. Generation of secondary vorticity in a stratified fluid. *Journal of Fluid Mechanics* **20**(2):177–181, 1964. <https://doi.org/10.1017/S0022112064001124>
- [18] A. W. Marris. Secondary flows in an incompressible fluid of varying density in a rotating reference frame. *Journal of Basic Engineering* **88**(2):533–537, 1966. <https://doi.org/10.1115/1.3645894>
- [19] A. W. Marris, S. L. Passman. Vector fields and flows on developable surfaces. *Archive for Rational Mechanics and Analysis* **32**(1):29–86, 1969. <https://doi.org/10.1007/BF00253256>
- [20] B. Lakshminarayana, J. H. Horlock. Generalized expressions for secondary vorticity using intrinsic co-ordinates. *Journal of Fluid Mechanics* **59**(1):97–115, 1973. <https://doi.org/10.1017/S0022112073001448>
- [21] J.-Z. Wu, H.-Y. Ma, M.-D. Zhou. *Vorticity and Vortex Dynamics*. Springer, 2006. <https://doi.org/10.1007/978-3-540-29028-5>
- [22] S. Zhang, D. Choudhury. Eigen helicity density: A new vortex identification scheme and its application in accelerated inhomogeneous flows. *Physics of Fluids* **18**(5):058104, 2006. <https://doi.org/10.1063/1.2187071>
- [23] E. Flídr, T. Jelínek, M. Kladrubský. Experimental investigation of effects of reynolds number and incidence angle on secondary flow within a linear blade cascade. *Journal of Thermal Science* **30**:1–15, 2021. <https://doi.org/10.1007/s11630-021-1455-y>
- [24] Y. Tang, Y. Liu. VR helicity density and its application in turbomachinery tip leakage flows. *Chinese Journal of Aeronautics* **35**(11):1–17, 2022. <https://doi.org/10.1016/j.cja.2022.05.006>